Table 1 Time to reach 100 AU (comparison with Sauer)

β	Closest distance from sun, AU	Time to reach 100 AU, years	
		Sauer[a]	Our current work
0.3	0.15	10	27.88[b]
0.3	0.2	11	16.79[b]
0.3	0.3	13	15.02
0.3	0.4	16	17.53
0.4	0.1	6.5	7.09
0.4	0.15	7.5	7.72
0.4	0.2	9	8.64
0.4	0.3	11	10.66
0.4	0.4	13	12.8
0.5	0.1	5.5	5.19
0.5	0.15	6.5	6.24
0.5	0.2	7.5	7.21
0.5	0.3	9.5	9.02
0.5	0.4	11.5	10.77
0.59	0.1	5.0	4.63
0.59	0.15	6	5.61
0.59	0.2	7	6.50
0.59	0.3	8.5	8.11
0.59	0.4	10.5	9.65
0.79	0.1	4.0	4.00
0.79	0.15	5.0	4.83
0.79	0.2	6	5.57

[a]These times were estimated from Fig. 8 in Ref. 3 using characteristic accelerations that correspond with β.
[b]Corresponds to trajectories that are stranded in large elliptical orbits.

V. Comparison with Sauer

We have compared our results with Sauer's time-optimal solar-sail trajectories to reach a particular distance.[3] We ran our simulations beyond escape and compared the time it took for our trajectories to reach 100 AU with those of Sauer. The results of this comparison can be found in Table 1. Sauer's globally optimized trajectories are found from satisfying the necessary conditions for optimality, whereas our trajectories follow an explicit guidance law. Surprisingly, this difference in approach has a relatively small effect on flight times in most cases. Although our locally optimal energy control law was not designed to minimize time to reach 100 AU, our flight times compare favorably with Sauer's optimized results. We note from Table 1 that for $\beta > 0.3$ the flight times of our trajectories get close to Sauer's and even surpass them, reaching 100 AU in less time. (This might be caused by having to interpolate Sauer's time-of-flight data from a plot.) This indicates that our control methodology is in some sense near optimal for some situations. Differences between our results arise when the trajectory following our law fails to achieve escape before reaching a highly elliptical orbit.

VI. Conclusions

This study explores the use of simple guidance laws that minimize or maximize orbit energy along a solar-sail trajectory to achieve escape conditions. We have established that maximizing the change in orbit energy at every instant along the trajectory does not necessarily minimize the time to escape. We found in general that first maximally decreasing energy and then maximally increasing energy leads to shorter escape times than escape trajectories that only maximally increase energy. These trajectories not only achieved escape in shorter time spans, but they also achieved escape using smaller values of β as compared with initially circular and elliptic trajectories. Using these controls, it is feasible to launch relatively poor performance solar sails ($\beta = 0.3$) into escape trajectories from the sun in less than one year. For high-performance sails ($\beta \geq 0.4$), the time to escape is insensitive to the energy minimizing/maximizing control strategy. Unlike most other works, we have focused on finding a general strategy for solar escape instead of designing trajectories for specific missions. Future research can begin with these simple controls to find generally applicable optimization strategies and can consider controls that maximize the final escape energy of the sail.

References

[1]Van der Ha, J. C., and Modi, V. J., "On the Maximization of Orbital Momentum and Energy Using Solar Radiation Pressure," *Journal of the Astronautical Sciences*, Vol. 27, No. 1, 1979, pp. 63–84.

[2]Leipold, M., and Wagner, O., "'Solar Photonic Assist' Trajectory Design for Solar Sail Missions to the Outer Solar System and Beyond," *Advances in the Astronautical Sciences*, Vol. 100, No. 2, 1998, pp. 1035–1045.

[3]Sauer, Carl G., Jr., "Solar Sail Trajectories for Solar Polar and Interstellar Probe Missions," *Advances in the Astronautical Sciences*, Vol. 103, Pt. 1, 2000, pp. 547–562.

[4]McInnes, Colin R., *Solar Sailing Technology, Dynamics, and Mission Applications*, Praxis Publishing, Ltd., Chichester, England, U.K., 1999, pp. 38–40, 112–169.

D. Spencer
Associate Editor

Simulation of Wind-Profile Perturbations for Launch-Vehicle Design

S. I. Adelfang*
Computer Sciences Corporation, Huntsville, Alabama 35815

Nomenclature

A_j, B_j	=	components of F_j
b	=	parameter for biasing an empirical gamma distribution, m/s
c	=	parameter in empirical model for mean normalized power spectrum density
E	=	variance coefficient of power-spectrum-density model, m^2/s^2
F_j	=	Fourier series, $\sqrt{[(m^2/s^2)/(m/s)]}$
n	=	wave number, 1/m
$r1_j$, $r2_j$	=	random number sequences that are tangents of j uniformly distributed random phase angles in the interval from $-\pi/2$ to $+\pi/2$
u and v	=	east–west and north–south wind components, respectively, m/s; sign convention eastward and northward wind positive
z	=	altitude, km
β	=	parameter of a gamma distribution, s/m
γ	=	parameter of a gamma distribution
σ	=	standard deviation of high-pass filtered wind profile, m/s

Introduction

IDEALLY, a statistically representative sample of measured high-resolution wind profiles with wavelengths as small as tens of meters is required in design studies to establish aerodynamic load indicator dispersions and vehicle control system capability.[1–3] At most potential launch sites, high-resolution wind profiles might not exist. Representative samples of relatively low-resolution Rawinsonde

Presented as Paper 2003-0896 at the 41st Aerospace Sciences Meeting, Reno, NV, 9–12 January 2003; received 20 June 2003; revision received 6 April 2004; accepted for publication 6 April 2004.

*Senior Computer Engineer; currently Senior Principal Scientist, Engineering/Science, Morgan Research Corporation, Huntsville, AL 35805-1948; stan.adelfang@msfc.nasa.gov. Member AIAA.

wind profiles to altitudes of 30 km are more likely to be available from the extensive network of measurement sites established for routine sampling in support of weather observing and forecasting activity. Such a sample, large enough to be statistically representative of relatively large wavelength perturbations, would be inadequate for launch-vehicle design assessments because the Rawinsonde system accurately measures wind perturbations with wavelengths no smaller than 2000 m (1000-m altitude increment). The Kennedy Space Center (KSC) Jimsphere[4–6] wind profiles (150/month and seasonal 2- and 3.5-h pairs) are the only adequate samples of high-resolution profiles (~150–300-m effective resolution, but oversampled at 25-m intervals) that have been used extensively for launch-vehicle design assessments. Therefore, a simulation process has been developed for enhancement of measured low-resolution Rawinsonde profiles that would be applicable in preliminary launch-vehicle design studies at launch sites other than KSC. The simulation of vertically nonhomogeneous horizontal gusts for enhancement of low-resolution wind profiles along the vertical was addressed in an earlier paper.[3] The simulation was based on stochastic models for two-point (in the vertical) covariance functions of gust components and models for the vertical variation of gust component standard deviation and gust length scale. This Note addresses the same objective with a different approach.

Simulation Process

The simulation process is based on a power-spectrum-density (PSD) model for wind-profile perturbations derived from samples of high-resolution KSC Jimsphere wind profiles. The magnitude of the simulated perturbations is established by assignment of the total perturbation energy to the simulated perturbation profile from a model based on KSC winter season perturbation data that tend to be more severe than in the other seasons. The seasonal and geographic variation of wind-profile perturbations with wavelengths less than 2000 m is unknown. Engineering application will require imposing a degree of conservatism that accounts for the uncertainty.

The model for the normalized PSD (NPSD) for wind component profile perturbations is of the form

$$\mathrm{NPSD}(n) \propto n^c \tag{1}$$

Normalization with respect to the variance produces a PSD that integrates to unity over the applicable wavelength range. The value of $c(-2.62)$ is derived from the mean NPSD (MNPSD) of each wind component (Fig. 1) calculated from 518 high-pass filtered KSC winter Jimsphere profiles. The high-pass filtered wind profile is the inverse transform of the truncated Fourier transform of the wind profile; harmonics for wavelengths greater than 2000 m are set equal to zero. The filtered wind profile has no spectral energy outside the wavelength range (50–2000 m) of the retained Fourier components and the Gibbs oscillation (filter transfer function side lobe noise) has not been detected. The line with slope minus 2.62 illustrated in Fig. 1 represents the form of the PSD model [Eq. (1)] that is a very good fit to the mean normalized PSD for wave number as large as 0.007 m^{-1} (~150-m wavelength) for the eastward wind component u and 0.0050 m^{-1} (~200-m wavelength) for the northward wind component v; the effective vertical resolution (EVR) of the Jimsphere system is defined by these wavelengths. The degradation of the Jimsphere system signal-to-noise ratio at higher wave numbers (inverse wavelength) is evidenced by the deviation of the MNPSD from the -2.62 slope illustrated in Fig. 1. These values of EVR (150 m for u and 200 m for v) based on analysis over the entire altitude range of the Jimsphere wind profiles are in general agreement with other studies.[6] High-altitude segments of Jimsphere profiles can have an EVR that can be as large as 300 m because the data-processing scheme of the Jimsphere system adjusts the data-smoothing interval as a function of detected noise level in the radar balloon tracking data, which tends to be larger at high altitudes and large slant ranges.[5]

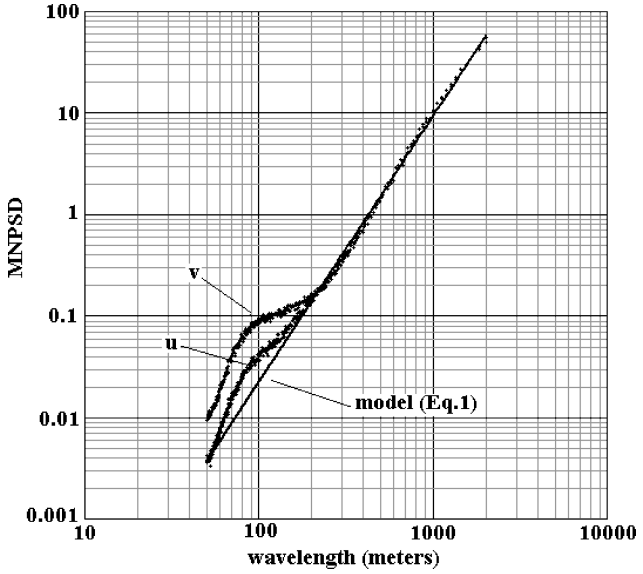

Fig. 1 Mean normalized PSD of 518 winter Jimsphere *u*- and *v*-component wind profiles and PSD model.

Application of the PSD model for simulation of wind-profile perturbations in the 50–2000-m wavelength range requires real and imaginary components, A and B of a Fourier series F to be uniquely defined for each simulation:

$$F_j = A_j + B_j i \tag{2}$$

In Eq. (2) j is the Fourier series harmonic index (1-400), and $i = \sqrt{-1}$. The values for A_j are B_j calculated from

$$A_j = \frac{\sqrt{\mathrm{PSD}_j}}{\sqrt{1 + r1_j^2}} \frac{r1_j}{|r1_j|}, \qquad B_j = \frac{\sqrt{\mathrm{PSD}_j}}{\sqrt{1 + r1_j^2 / r1_j^2}} \frac{r2_j}{|r2_j|} \tag{3}$$

where the PSD of each wind component is

$$\mathrm{PSD}_j = A_j^2 + B_j^2 \tag{4}$$

and $r1_j$ is a random number sequence that is the tangent of j uniformly distributed random phase angles in the interval from $-\pi/2$ to $+\pi/2$. The random number $r2_j$ is also uniformly distributed within equal intervals on either side of zero. The quantities $r1_j/|r1_j|$ and $r2_j/|r2_j|$ ensure that the random phase at each harmonic can be in any quadrant. A unique set of j values of $r1$ and $r2$ are generated for each simulated wind profile. Thus, each simulated wind perturbation profile is uniquely determined by its unique random phase distribution. The justification for random phase is established from analysis of the Jimsphere wind-profile phase spectrum. The phase distribution determines how the Fourier components combine to produce a unique simulated time series, for an invariant PSD at each harmonic. Note that the PSD in Eqs. (3) and (4) is not normalized, that is, it is of the form

$$\mathrm{PSD}(n) = En^c \tag{5}$$

Parameter E is set such that a desired value of the variance is obtained when the PSD function is integrated over the wave-number range (1/2000–1/50 m^{-1}). The units of PSD are variance per wave-number interval, which for this study is $\{(\mathrm{m}^2/s^2)/(1/m)\}$. The final step in the simulation process is to generate the simulated time series by calculating the inverse Fourier transform of F_j. Two sets of values for the series F_j, calculated from A_j and B_j [Eqs. (2) and (3)] are required: one set for each wind component. The variance of each simulated wind component perturbation profile is adjusted to a value obtained by random selection from an empirical gamma probability distribution of standard deviation σ_n (square root of variance) derived from the 518 KSC winter high-pass wind component profiles. The gamma probability density functions in the 50–2000-m wavelength range are of the form

$$\sigma(\beta, \gamma) = [\beta^\gamma / \Gamma(\gamma)](y - b)^{\gamma - 1} \exp[-\beta(y - b)] \tag{6}$$

Table 1 Parameters β, γ, and b of gamma distributions for u and v wind component perturbation standard deviation σ

Wind component	β, s/m	γ	b, m/s
u	12.13	12.43	0.42
v	6.89	5.31	0.90

where β and γ are estimated from sample statistics of σ for each wind component and b is an empirically derived bias parameter that ensures the best fit to the observed distribution[7]:

$$\gamma = \left(\frac{\text{mean}(\sigma - b)}{\text{stdev}(\sigma - b)}\right)^2 \beta = \frac{\gamma}{\text{mean}(\sigma - b)} \tag{7}$$

The values for β, γ, and b are listed in Table 1. The theoretical cumulative gamma probability functions for wind component standard deviations (50–2000-m wavelength band) are derived by integration of Eq. (6) from a lower limit of zero to any desired value y for σ.

The simulated wind component perturbation profiles are adjusted such that the variation of component standard deviation as a function of altitude observed in the original sample of 518 high-pass filtered Jimsphere wind component profiles is reproduced in the simulated profiles.[7] To address a concern that the high-pass filtered wind component standard deviation illustrated can be unduly influenced at high altitudes by Jimsphere tracking system noise and data gaps, the standard deviations were also calculated from a sample of 26 high-resolution Automated Meteorological Profiling System (AMPS) wind profiles.[8] The AMPS wind measurement error is not sensitive to balloon azimuth and altitude because it is based on global positioning system tracking for determination of balloon position and calculation of wind vectors along the balloon trajectory. The standard deviations from this relatively small sample of AMPS profiles obtained during a five-month period exhibit the same behavior derived from the larger Jimsphere winter sample. The empirical function derived from the Jimsphere sample also fits the AMPS variation.[7]

The enhancement process is completed by adding a unique simulated wind component perturbation profile to each Rawinsonde wind component profile that has been cubic-spline interpolated to the same altitude interval (25 m) as the simulated profile.[7]

Summary

Detailed wind profiles that are statistically representative at a selected launch site are a critical requirement in design studies to establish vehicle structural integrity and program risk for vehicle operations within the range of detailed wind-profile variability. A methodology has been developed for simulation of wind-profile perturbations in a prescribed wavelength band. These perturbation profiles to wavelengths as small as tens of meters are appended to statistically representative low-resolution Rawinsonde wind-profile databases that are likely to be available at or near candidate launch sites. The simulation process is based on the inverse transform of the Fourier series having random components that define the PSD and the uniformly distributed phase angles of the Fourier harmonics. The PSD model for wind-profile perturbations is derived from a large sample (518) of Jimsphere detailed wind profiles. Profiles so derived are a reasonable choice for initial launch-vehicle design studies. Once a launch site is selected, it would be prudent to establish a wind-profile measurement program based on Jimsphere or its equivalent to obtain a statistically representative sample of detailed wind profiles. As the development process continues toward commitment to hardware production, the vehicle design originally based on enhanced Rawinsonde profiles could be assessed with the launch site high-resolution wind profiles.

Acknowledgment

This study was performed for the Marshall Space Flight Center under the Program Information Systems Mission Services Contract (NAS8-6000).

References

[1]Sako, B. H., Kim, M. C., Kabe, A. M., and Yeung, W. K., "Derivation of Atmospheric Gust-Forcing Functions for Launch-Vehicle Loads Analysis," *Journal of Spacecraft and Rockets*, Vol. 37, No. 4, 2000, pp. 434–442.

[2]Adelfang, S. I., Smith, O. E., and Batts, G. W., "Ascent Wind Model for Launch Vehicle Design," *Journal of Spacecraft and Rockets*, Vol. 31, No. 3, 1994, pp. 502–508.

[3]Fichtl, G. H., and Perlmutter, M., "Stochastic Model of Vertically Nonhomogeneous Gusts," *Journal of Spacecraft and Rockets*, Vol. 13, No. 10, 1976, pp. 577, 578.

[4]Wilfong, T. L., and Boyd, B. F., "Winds Aloft to Support Space and Missile Launches," *Proceedings of the Third International Conference on the Aviation Weather System*, American Meteorological Society, Boston, 1989, pp. 102–107.

[5]Wilfong, T. L., Smith, S. A., and Crosiar, C. L., "Characteristics of High Resolution Wind Profiles Derived from Radar Tracked Jimspheres and the Rose Processing Program," *Journal of Atmospheric and Oceanic Technology*, Vol. 14, No. 4, 1997, pp. 318–325.

[6]Johnson, D. (ed.), "Terrestrial Environment (Climatic) Criteria Handbook for Use in Aerospace Vehicle Development," NASA HDBK-1001, 11, Aug. 2000.

[7]Adelfang, S. I., "Simulation of Wind Profile Perturbations for Launch Vehicle Ascent Flight Systems Design Assessments," AIAA Paper 2003-0896, Jan. 2003.

[8]Wilfong, T. L., Maier, M. L., Crosiar, C. L., Hinson, M. S., and Divers, B., "Characteristics of Wind Profiles Derived from GPS Based Automated Meteorological Profiling System (AMPS)," Ninth Conf. on Aviation, Range and Aerospace Meteorology, Paper J8.2, American Meteorological Society, Boston, 2000.

C. Kluever
Associate Editor

Analytical Methods for Predicting Grain Regression in Tactical Solid-Rocket Motors

Roy Hartfield,* Rhonald Jenkins,* John Burkhalter,† and Winfred Foster†
Auburn University, Auburn, Alabama 36849-5338

Introduction

In many practical solid-rocket-motor design efforts, final geometric designs for grains are arrived at using numerical layering techniques. This process is geometrically versatile and imminently practical for cases where small numbers of final geometries are considered. However, for a grain-design-optimization process where large numbers of grain configurations must be considered, the generation of grids for each candidate design is often prohibitive. For such optimization processes, analytical developments of burn perimeter and port area for two-dimensional grains are critically important.[1] Most modern rocket-propulsion texts do not provide geometric details for grain design.[2,3]

Analytical developments for solid-rocket-motor grains were much more prevalent in the decades before widespread use of microcomputers. A summary of one version of the burnback equations for the star grain and for part of one type of wagon wheel can be found

Received 17 June 2003; presented as Paper 2003-4506 at the AIAA/ASME/SAE/ASEE 39th Joint Propulsion Conference, Huntsville, AL, 20–23 July 2003; revision received 10 September 2003; accepted for publication 10 September 2003.

*Associate Professor, Aerospace Engineering Department. Member AIAA.

†Professor, Aerospace Engineering Department. Member AIAA.